

Reduction of Structural Vibrations by Passive and Semi-Actively Controlled Friction Dampers

Jens Becker and Lothar Gaul

Abstract Reduction of structural vibrations is of major interest in mechanical engineering for lowering sound emission of vibrating structures, improving accuracy of machines and increasing structure durability. Besides optimization of the mechanical design or various types of passive damping treatments, active structural vibration control concepts are efficient means to reduce unwanted vibrations.

In this contribution, two different semi-active control concepts for vibration reduction are proposed that adapt the normal force of attached friction dampers. Thereby, semi-active control concepts generally possess the advantage over active control that the closed loop is intrinsically stable and that less energy is required for the actuation than in active control. In the chosen experimental implementation, a piezoelectric stack actuators is used to apply adjustable normal forces between a structure and an attached friction damper. Simulation and experimental results of a benchmark structure with passive and semi-actively controlled friction dampers are compared for stationary narrow-band excitation.

For simulations of the control performance, transient simulations must be employed to predict the achieved vibration damping. It is well known that transient simulation of systems with friction and normal contact requires excessive computational power due to the nonlinear constitutive laws and the high contact stiffnesses involved. However, commercial finite element codes do not allow to simulate feedback control in a general way. As a remedy, a special simulation framework is developed which allows to efficiently model interfaces with friction and normal contact by appropriate constitutive laws which are implemented by contact elements in a finite element model. Furthermore, special model reduction techniques using a substructuring approach are employed for faster simulation.

Jens Becker · Lothar Gaul

Institut für Angewandte und Experimentelle Mechanik, Universität Stuttgart, e-mail: becker@iam.uni-stuttgart.de, e-mail: gaul@iam.uni-stuttgart.de

1 Introduction

Semi-active control strategies for vibration reduction offer interesting alternatives to passive means of damping enhancement or fully active vibration control (AVC). Hereby, the term semi-active means that passive system properties, such as friction, material damping or fluid viscosity, are actively controlled. This intrinsically eliminates the problem of system destabilization due to spillover effects encountered in AVC applied to flexible structures [1, 4]. Furthermore, semi-active control is more energy-efficient than fully active ones in general which is an important aspect from an application point of view. In exchange of these advantages, the achievable performance is limited by the effectiveness of the underlying passive damping mechanism. Though, they outperform passive vibration reduction means due to their ability to adapt to the instantaneous vibration state of the structure. This property links semi-active control concepts to the research area of smart/adaptive structures and adaptronics. Advantages over fully active control are that semi-active control is inherently fail-safe, guarantees stability and introduces significant passive damping into the mechanical system, e.g. by the attached friction damper in this contribution.

Semi-active control concepts are probably most often applied to magneto- or electrorheological dampers, friction damping devices or actively tuned absorbers with variable-stiffness dampers, see [11, 6, 3, 10, 9] for some examples. The specific idea of using friction in joints for vibration damping by normal force control is reported first in [7], which subsequently inspired several researchers, see e.g. [8].

In this contribution, two control algorithms for the semi-active vibration control of the normal force between a main structure and attached damper exploiting dry friction damping are investigated.

Generic Benchmark Structure

A beam-like friction damper element is attached to a beam-like metal benchmark structure by a normal screw and an adaptive screw. The principle is depicted schematically in Fig. 1, a picture of the experimental realization is shown in Fig. 2. The screw $F_{N,2}$ is strongly tightened ($F_{N,2} = 6000$ N) whereas the normal force $F_{N,1}$ of the adaptive screw can be controlled by means of a piezoelectric ring stack actuator. For that purpose, the control measures the acceleration close to the tip.

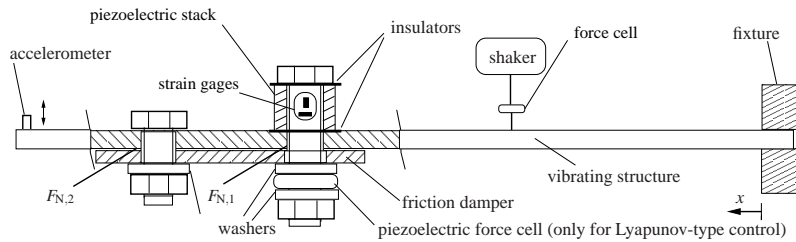


Fig. 1 Sketch of the benchmark structure (steel, 775 mm length, 40 mm width, 3 mm thickness) with adaptive friction damper beam (steel, 160 mm length, 40 mm width, 3 mm thickness).

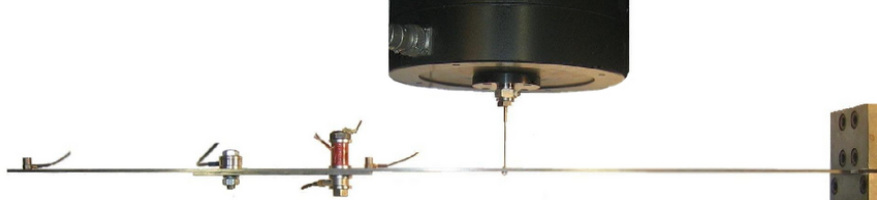


Fig. 2 Photograph of the experimental setup with structure, damper beam, piezoelectric stack, force cell, accelerometers and attached shaker stinger (cf. Fig. 1)

2 Finite-Element Modeling

The structure is discretized by the finite-element (FE) method and node-node contact elements for the normal and tangential contact (Fig. 3). In a generic way, the discretized structural dynamics of the two substructures, namely the main structure and the attached friction damper beam, is given as

$$\begin{bmatrix} M^{(1)} & 0 \\ 0 & M^{(2)} \end{bmatrix} \ddot{x} + \begin{bmatrix} K^{(1)} & 0 \\ 0 & K^{(2)} \end{bmatrix} x + \begin{bmatrix} B_T^{(1)} \\ B_T^{(2)} \end{bmatrix} F_T^c + \begin{bmatrix} B_N^{(1)} \\ B_N^{(2)} \end{bmatrix} F_N^c = B \begin{bmatrix} F_{N,1} \\ F_{N,2} \end{bmatrix} + F_{\text{exc}}, \quad (1)$$

where the nodal normal contact forces F_N^c and tangential friction forces F_T^c act as internal forces on the contact interface between main structure and damper beam. On the right-hand side, the external forces appear, namely the two pairs of clamping forces $F_{N,1}, F_{N,2}$ and dynamic excitation loads F_{exc} (later, $F_{N,1}$ is controlled).

Constitutive equations are implemented for the normal contact and the tangential contact in the interface by node-to-node contact elements. The former is a bilinear stiffness relationship that allows separation but penalizes penetration. The latter is an elasto-plastic friction law, which can be seen as two dimensional version of a Jenkins element model depicted in Fig. 4 for the one-dimensional case, i.e. a series combination of a spring and a Coulomb element.

The nonlinear system of Eq. 1 is solved with the Newmark scheme and Newton equilibrium iterations at each fixed time step. Beforehand, substructure model reduction techniques are employed to reduce the dimensions of the system. For that purpose, an in-house simulation tool [2] is developed to facilitate general feedback control simulation, which is not supported by commercial FE codes.

The model parameters including the contact parameters are updated by comparison of experimentally and numerically obtained FRFs (frequency response function) with impulse hammer excitation that cover a large range of constant clamping forces. An exemplary FRFs is shown in Fig. 5 where the nonlinear effects become visible by some unsymmetric peak forms (e.g. at 230 Hz) and some higher harmonics peaks. From the FRF, the damping ratios are identified for the bending modes, see Fig. 5. They show good agreement between simulation and experiment and that significant damping is introduced by the friction damper if they are compared to the modal damping ratios of less than 0.15% found without attached damper.

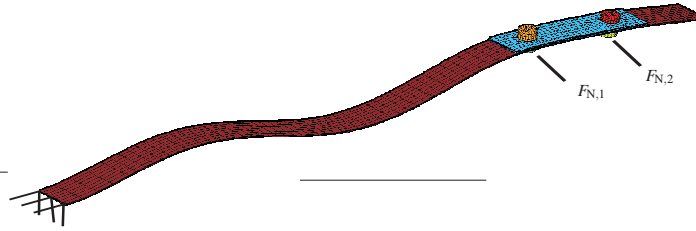


Fig. 3 Finite-element model (≈ 30000 DOFs and 632 nodes in contact) in typical bending deformation with the two screws that impose the external clamping force pairs $F_{N,1}$ and $F_{N,2}$.

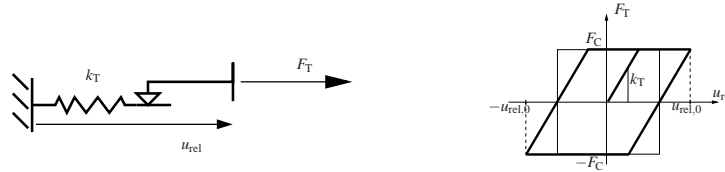


Fig. 4 1-D Jenkins friction model and its hysteresis loop (thick) in comparison to the Coulomb friction hysteresis (thin). Note, that for increasing tangential stiffness, the hysteresis approximates the Coulomb model hysteresis.

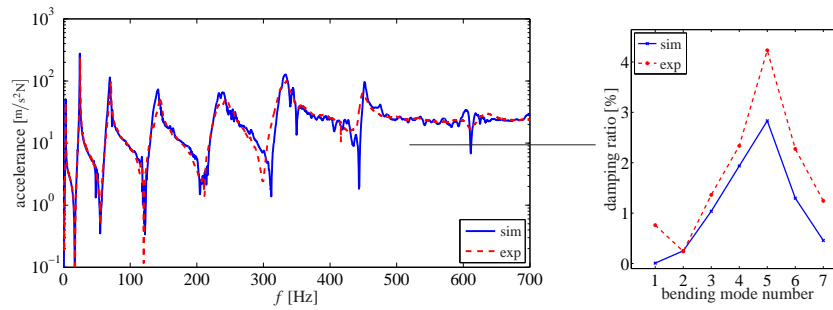


Fig. 5 Measured and simulated FRFs for impulse excitation and $F_{N,1} = 100$ N, $F_{N,2} = 6000$ N (excitation and measurement close to tip on the mid-axis) and determined modal damping ratios.

3 Semi-active Vibration Control

Two controllers each consisting of an appropriate nonlinear control law plus an observer to estimate non-measurable variables required by the control are introduced in the following. The first control is denoted hysteresis-optimal control and is motivated by experimental investigations. They show that relatively simple dynamical friction models are often capable to model the most dominant friction effects in structures with local joints [5]. Among others, the Jenkins element as depicted in Fig. 4, has proven its usability for that purpose and serves as base for the control derivation.

Hysteresis-optimal Control

For that, it is assumed that the dominant damping effects are located in the contact area close to the adaptive screw and can be modeled by a discrete friction model. Then, the dissipated work W_d due to friction during one vibration cycle is maximized to find the control. For the chosen model, the dissipated energy

$$W_d = 4 \left(u_{\text{rel},0} - \frac{F_C}{k_T} \right) F_C \quad \text{with} \quad F_C = \mu F_N \quad (2)$$

is maximized to yield the optimal normal force F_N as a function of the tangential contact stiffness k_T , the friction coefficient μ and the relative sliding oscillation amplitude $u_{\text{rel},0}$

$$F_N = f(u_{\text{rel},0}) = \frac{k_T u_{\text{rel},0}}{2\mu} = k_T^* u_{\text{rel},0}. \quad (3)$$

Note that similar algebraic expressions could be derived also based on hysteresis loops of more complex friction models involving more parameters. Eq. 3 is interpreted as control law to adjust the normal force $F_N = F_{N,1}$ according to Fig. 1 to the structural vibration tangential amplitude. The required actual vibration displacement amplitude $u_{\text{rel},0}$ can be found under the assumption of mono-frequent displacement (with zero mean) by $u_{\text{rel},0} \approx \frac{\pi}{2T} \int_{t-T}^t |u_{\text{rel}}| \, d\tau$ from the estimated signal u_{rel} . The evaluation of the integral would need large memory storage for the required integration time much larger than the largest vibration period of interest, hence it is efficiently approximated by a PT₁ element, where the time constant T_1 prescribes how fast the signal $u_{\text{rel},0}$ follows a change in the vibration amplitude

$$T_1 \dot{u}_{\text{rel},0} + u_{\text{rel},0} = \frac{\pi}{2} |u_{\text{rel}}|. \quad (4)$$

Model-based Design of Nonlinear Observer

In general, the required tangential displacement u_{rel} at the adaptive screw can not be measured which makes the design of a nonlinear observer necessary which estimates it from available measurements such as displacements, strains or accelerations and a simplified approximate simulation model (without having any information about the excitation forces).

This model is derived by rigid connection of the damper beam at one end ($F_{N,2}$) and neglectation of the normal contact between damper and base structure, instead appropriate spring elements are introduced in normal direction in some distance around the adaptive screw. The relative motion at the adaptive screw is used for the output definition of \hat{u}_{rel} . The nonlinear observer is of the form

$$\begin{aligned} \dot{\hat{z}} &= A \hat{z} + B_T f_{\text{friction}}(\hat{F}_T, \hat{u}_{\text{rel}}, F_N) + B_{\text{exc}} F_{\text{exc}} + l(y_{\text{meas}} - \hat{y}_{\text{meas}}), \\ \text{with } \hat{y}_{\text{meas}} &= C \hat{z} \quad \text{and} \quad \hat{u}_{\text{rel}} = C_{\text{rel}} \hat{z}. \end{aligned} \quad (5)$$

Hereby, the the measurement output y_{meas} denotes the velocity measurement obtained by integration of the acceleration in the experiment. The estimated output

\hat{u}_{rel} replaces the required variable u_{rel} by the nonlinear control law (Eq. 3). A simple dynamic friction model $f_{\text{friction}}(\cdot)$ is used to model the friction F_{T} at the adaptive screw, namely a regularized Coulomb friction model

$$F_{\text{T}} = f_{\text{friction}}(\hat{u}_{\text{rel}}, F_{\text{N}}) = \mu F_{\text{N}} \frac{2}{\pi} \arctan(\alpha \hat{u}_{\text{rel}}), \quad (6)$$

which depends on the relative velocity \hat{u}_{rel} with the regularization parameter α determined by simulation studies. Theoretically, the use of more complex dynamic friction models would be of interest, the hard real-time limitations imposed by the fixed-step time-integration in the experiment and the considered high frequencies forbids their application for the investigated problem. The obtained estimation accuracy has been verified in simulations that are also used to optimize the observer. The linear system parts in Eq. 5 are obtained from an simplified, linear FE model after modal truncation plus a static correction step for the transfer path between F_{T} and \hat{u}_{rel} . With the required output variables, mass and stiffness matrices M, K and load vector F_{exc} , this simplified model reads

$$M\ddot{x} + Kx + F_{\text{I}} = \beta_{\text{exc}} F_{\text{exc}}, \quad y_{\text{meas}} = \gamma_{\text{meas}} x \quad \text{and} \quad u_{\text{rel}} = \gamma_{\text{rel}} x. \quad (7)$$

Solving the associated eigenvalue problem $(K - \omega^2 M)\phi = 0$ yields the eigenfrequencies ω_k and eigenvectors $\phi_k (k \in \mathbb{N}^+)$ which allows a modal truncation to the first N important bending modes by the transformation $x = T x^*$ with $T = [\phi_1, \phi_2, \dots, \phi_N]$. This transforms the system matrices, $I = T^{\text{T}} K T$ and $\Omega = T^{\text{T}} K T = \text{diag}\{\omega_1^2, \omega_2^2, \dots, \omega_N^2\}$, as well as the other matrices in Eq. 5. With the state vector $z^{\text{T}} = [\dot{x}^{*\text{T}}, x^{*\text{T}}]$ and some damping matrix Δ , these linear system parts read

$$A = \begin{bmatrix} -\Delta & -\Omega \\ I & 0 \end{bmatrix}, \quad B_{\text{T}} = \begin{bmatrix} -\Theta^{\text{T}} \gamma_{\text{rel}}^{\text{T}} \\ 0 \end{bmatrix}, \quad B_{\text{exc}} = \begin{bmatrix} \Theta^{\text{T}} \beta_{\text{exc}} \\ 0 \end{bmatrix} \quad (8)$$

$$C_{\text{rel}} = [0, \gamma_{\text{rel}} \Theta], \quad C_{\text{meas}} = [0, \gamma_{\text{meas}} \Theta], \quad (9)$$

After linearization around $u_{\text{rel}} = 0, F_{\text{N}} = 0$, the observer gains l in Eq. 5 are determined by a Kalman design procedure from the solution of the associated Riccati equation for appropriate state and measurement noise variance matrices. The obtained control loop is shown in Fig. 6.

Lyapunov-type Control

For the second proposed control law, Lyapunov's direct method is applied by choosing the mechanical system energy as Lyapunov function $V(x)$ and under the assumption of a discrete friction model with controlled normal force [8]. It is imposed that its time derivative $\dot{V}(x)$ must be semi-negative, which is directly related to the differential form of the passivity condition. Its absolute value is furthermore maximized for optimality in the Lyapunov sense. Recalling the dynamics of a 1-DOF system

$$m \ddot{u}_{\text{rel}} + k u_{\text{rel}} + F_{\text{T}} = 0, \quad (10)$$

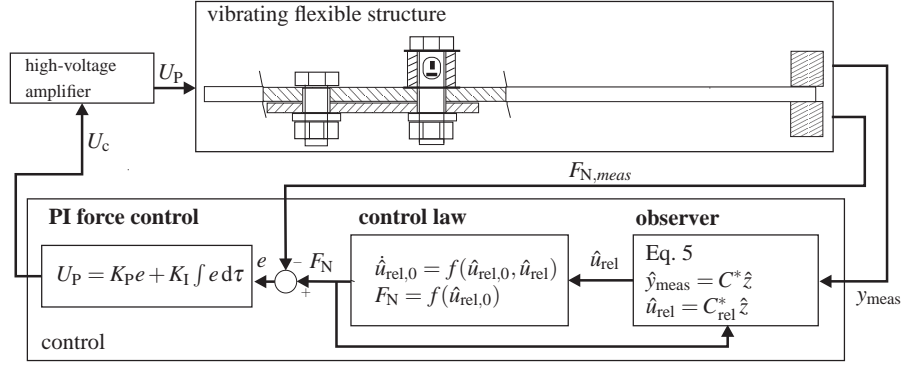


Fig. 6 Closed control loop with hysteresis-optimal control law.

the passivity condition in terms of the friction force F_T and the relative velocity \dot{u}_{rel}

$$F_T \dot{u}_{rel} \geq 0 \quad \forall t \quad (11)$$

ensures a power flow outwards of the controlled structure. To enforce Eq. 11, a control law based on a Jenkins friction model must depend on the actual friction force F_T . However, in practice, for structures as the investigated one it is almost impossible to measure or estimate this force because of the distributed friction interface and the high stiffnesses in combination with the hard real-time constraints. Hence, the Coulomb friction model according to $F_T = \mu F_N \text{sign}(\dot{u}_{rel})$ is assumed as a good approximation instead. For this, it can be shown that a velocity-dependent bang-bang controller is optimal in the Lyapunov sense [8], $F_N = 0$ for $|\dot{u}_{rel}| = 0$ and $F_N = F_{N,max}$ for $|\dot{u}_{rel}| \geq 0$. This approach is appropriate in view of the high values for the tangential stiffness k_T found in the model updating before. Additional regularization with a boundary layer ε to avoid chattering effects and introduction of the minimal normal force yields the sub-optimal law

$$F_N = \begin{cases} \max\left\{\frac{|\dot{u}_{rel}|}{\varepsilon} F_{N,max}, F_{N,min}\right\} & \text{for } |\dot{u}_{rel}| < \varepsilon \\ F_{N,max} & \text{for } |\dot{u}_{rel}| \geq \varepsilon \end{cases} \quad (12)$$

Again, the required tangential relative motion must be estimated by the previously introduced observer which now estimated the relative velocity \dot{u}_{rel} instead of the displacement u_{rel} . Note that the minimal and maximal normal forces $F_{N,min}$ and $F_{N,max}$ are determined by the mechanical properties of the adaptive screw.

4 Experiments and Simulation Results

The proposed controls are investigated for the benchmark structure with a damper beam at $x_d = 0.545$ m away from the fixture. For this position, significant relative

displacement between structure and damper is expected for the bending modes 3, 4 and higher. For mode 2, much less relative motion is expected which explains the small damping values obtained in the experiment and simulations, e.g. for the passive results in Fig. 5. The first mode is not considered because it can not be excited by the available shaker. For evaluation, acceleration FRFs from the excitation force (at $x = 0.325$ m) to the measured acceleration (at $x = 0.45$ m) are compared.

Controller Implementation

A *dSpace* system running at 21 kHz sampling frequency is used for the real-time implementation. The observer is designed based on 7 normal modes and uses the out-of-plane tip acceleration at $x = 0.765$ m as measurement variable y_{meas} .

In the experiment, the prescribed force F_N for the adaptive screw from Eq. 3 or Eq. 12 must be tracked by an underlying force feedback control loop to compensate nonlinearities, large-signal piezoelectric effects, creep effects in the screw threads as well as to decrease the inertia forces of the actuator and sensor masses due to the structural vibrations. For that, a tracking controller is employed which is combined from a feedforward term derived from the static actuator voltage-force relationship and a PID feedback control of the measured force. The obtained actuator signal U_P is filtered by a 30 kHz low-pass to decrease the digitization noise before it is amplified for the piezoelectric stack actuator. To maximize the stiffness of the clamping of the piezoelectric actuators determining the achievable stroke [4], strain gages directly embedded in the bolt shaft (see Fig. 6) measure the actual force instead of strain-gage based ring force cells that would significantly weaken the configuration. The applicable actuator stroke lies between $F_{N,\text{min}} = 40$ N and $F_{N,\text{max}} \approx 600$ N.

For the Lyapunov-type control, a piezoelectric force cell of high sensitivity and bandwidth is added (cf. Fig. 2) because its high actuation dynamics requires a very high control bandwidth which is difficult to realize with strain-gage based force measurements due to the found signal-to-noise ratio and delays originating from the necessary amplifiers.

Shaker Test Setup with Excitation Force Control

For nonlinear mechanical structures, comparing FRFs requires special care because the obtained FRFs are nonlinear. More specifically, their resonance frequencies, peak amplitudes and peak forms depend on the excitation signal as well as amplitudes. Consequently, the amplitude is controlled during sine sweep measurements to make the excitation independent of the structural impedance for consistent comparisons. Very low sweep velocities (0.1 Hz/s) are employed to obtain steady-state conditions which approximates step-sine testing and to avoid interaction between the interesting effects of the semi-active structural control and the shaker control. Due to the very small relative displacements outside resonances, the control is only effective close to resonances which allows to restrict the evaluation around the resonance frequencies to save simulation and measurement time.

In Figs. 7 to 8, FRFs with and without semi-active control are shown for some typical excitation amplitudes for the two control concepts. Similar results are obtained

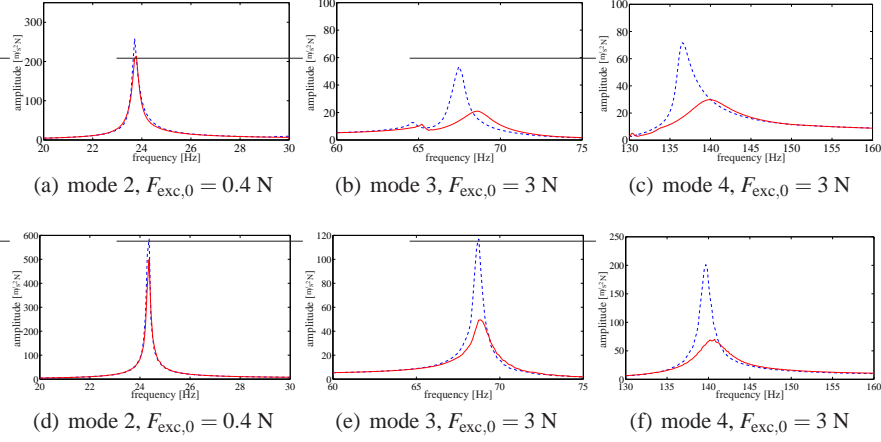


Fig. 7 hysteresis-optimal control: Measured (top) and simulated (bottom) acceleration FRFs for controlled sine-sweep excitation with (solid) and without (dashed) control ($k_T^* = 2.5 \cdot 10^7 \text{ N/m}$).

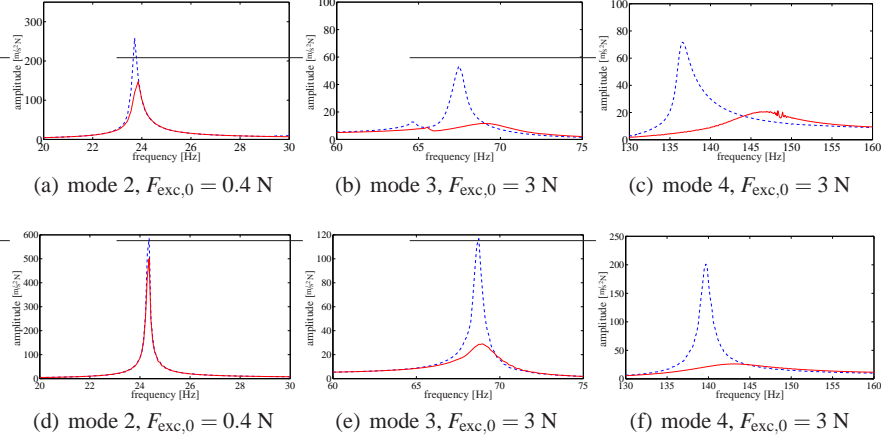


Fig. 8 Lyapunov-type control: Measured (top) and simulated (bottom) acceleration FRFs for controlled sine-sweep excitation with (solid) and without (dashed) control ($\varepsilon = \frac{1}{200} \text{ m/s}$).

for other amplitudes. It can always be seen that the control strongly reduces the resonance amplitudes of multiple modes. Note that in the passive case, the minimal possible force $F_N = F_{N,\text{min}}$ is applied to the adaptive screw which still introduces significant structural damping compared to the case without attached damper. Experiments and simulation additionally prove that the semi-active control never decreases the passive damping effect at lower excitation amplitudes. Generally, the agreement obtained between experiment and simulations is rated very good in view

of the well-known difficulties encountered in the prediction of nonlinear damping of structures, especially for distributed friction with inhomogeneous normal contact pressure distribution. Furthermore some imperfections of the excitation control can not be avoided as well as some changes in the contact parameters. The Lyapunov-type control achieves higher vibration reduction than the hysteresis-optimal in both experiments and simulations, especially at smaller vibration amplitudes. It is also suited to suppress broadband vibrations, is relatively robust to errors in the estimation but, as a drawback, its high-dynamical actuation requires more power. Advantageously, the hysteresis-optimal control could be implemented with low dynamical actuators, e.g. of different actuation principles.

5 Conclusion

Multi-modal, semi-active vibration controllers that adapt the normal force applied to friction damper beams by piezoelectric stack actuators are investigated for a generic benchmark structure in experiments and simulations. They are shown to efficiently damp structural resonances for different excitation amplitudes and vibration modes.

Which of the investigated controller concepts suits best for a certain application depends mainly on the actuator principle, the power considerations and if the excitation is rather broadband or narrowband.

Acknowledgements The support of the DFG (German Research Foundation) with project SPP 1156 is gratefully acknowledged.

References

1. Balas, M.: Feedback control of flexible systems. *IEEE Trans. Automatic Control* **23**(4), 673–679 (1978)
2. Becker, J., Gaul, L.: CMS methods for efficient damping prediction for structures with friction. In: *Proc. of the IMAC-XXVI*. Orlando, Florida USA (2008)
3. Dupont, P., Kasturi, P., Stokes, A.: Semi-active control of friction dampers. *Journal of Sound and Vibration* **202**(2), 203–218 (1997)
4. Fuller, C., Elliott, S., Nelson, P.: *Active Control of Vibration*. Academic Press (1996)
5. Gaul, L., Nitsche, R.: Role of friction in mechanical joints. *Appl. Mechanics Rev.* **54**, 93–105 (2001)
6. Jansen, L.M., Dyke, S.J.: Semi-active control strategies for MR dampers: A comparative study. *ASCE Journal of Engineering Mechanics* **126**(8), 795–803 (2000)
7. Lane, J.S., Ferri, A.A., Heck, B.S.: Vibration control using semi-active friction damping. In: *Proceedings of the Winter Annual Meeting of the ASME*, vol. 49, pp. 165–171 (1992)
8. Nitsche, R., Gaul, L.: Lyapunov design of damping controllers. *Archive of Applied Mechanics* **72**, 865–874 (2003)
9. Nitzsche, F., Zimcik, D.G., Wickramasinghe, V.K., Yong, C.: Control laws for an active tunable vibration absorber designed for rotor blade damping augmentation. *Aeronautical Journal* **108**(1079), 35–42 (2003)
10. Patten, W.N., Mo, C., Kuehn, J., Lee, J.: A primer on design of semiactive vibration absorbers (sava). *ASCE Engineering Mechanics* **124**(1), 61–68 (1998)
11. Symans, M.D., Constantinou, M.C.: Seismic testing of a building structure with a semi-active fluid damper control system. *Earthquake Eng. and Structural Dynamics* **26**, 759–777 (1997)